



## Far-reaching transient motions after Mojave earthquakes require broad mantle flow beneath a strong crust

Andrew M. Freed,<sup>1</sup> Roland Bürgmann,<sup>2</sup> and Thomas Herring<sup>3</sup>

Received 18 June 2007; revised 27 August 2007; accepted 30 August 2007; published 2 October 2007.

[1] Geodetically observed postseismic surface displacements in the 7 years following the 1999 Hector Mine earthquake demonstrate a previously unrecognized broad pattern of transient deformation throughout southern California and into Nevada, more than 200 km from the epicenter. Unlike previous postseismic observations in which trade-offs between postseismic mechanisms and the depth of flow lead to non-unique solutions, this deformation pattern can only be explained by viscoelastic flow in a region of the mantle 100s of km wide and below a depth of 40 km. This result enables two robust conclusions regarding the nature of lithospheric strength in this region: the mantle is weaker than the lower crust, and flow occurs over a wide region of mantle as opposed to within a narrow shear zone beneath the fault. **Citation:** Freed, A. M., R. Bürgmann, and T. Herring (2007), Far-reaching transient motions after Mojave earthquakes require broad mantle flow beneath a strong crust, *Geophys. Res. Lett.*, 34, L19302, doi:10.1029/2007GL030959.

### 1. Introduction

[2] The variation of strength with depth of continental lithosphere is much debated. Depending on the composition and water content of the lower crust, warm temperatures may lead to a weak viscously deforming layer sandwiched between strong upper-crustal and upper-mantle layers; i.e. a “jelly sandwich” structure [e.g., *Chen and Molnar*, 1983]. Hotter temperatures in the mantle combined with a higher water content could, however, cause the upper mantle to be weaker than the lower crust; i.e. a “crème brûlée” structure [*Jackson*, 2002; *Burov and Watts*, 2006]. It also continues to be a question of much debate if continental deformation at depth occurs along discrete, strain-weakened shear zones or is distributed in viscously deforming lower crust and lithospheric mantle. Because of the difficulty to directly determine viscoelastic strength and the degree of localization of deformation in the lower crust and upper mantle, there is no consensus on which region contributes most to the strength of the lithosphere and how this may vary with tectonic regime, crustal age or other factors.

[3] A useful approach for inferring the strength of the lithosphere is to utilize earthquakes as large rock deformation experiments where coseismic stress changes induce a variety of postseismic responses, including afterslip, poro-

lastic rebound, and viscoelastic relaxation. Each of these mechanisms is capable of inducing observable postseismic surface deformation that can constrain numerical models to help understand the rheological properties of the lithosphere. Given the limited spatial and temporal resolution of postseismic observations, however, it has proven difficult to sort out the relative contributions of each mechanism, let alone to determine how viscosity varies as a function of depth. Consider the interpretation of postseismic deformation following the 1992 M7.3 Landers earthquake in the Mojave Desert. Studies have inferred only afterslip [*Shen et al.*, 1994], only viscoelastic relaxation in the lower crust [*Deng et al.*, 1998]; viscoelastic relaxation predominately in the upper mantle [*Pollitz et al.*, 2000; *Freed and Bürgmann*, 2004], a combination of poroelastic rebound and afterslip [*Peltzer et al.*, 1998; *Fialko*, 2004a], or a combination of poroelastic rebound and viscoelastic relaxation in the lower crust [*Masterlark and Wang*, 2002]. The various conclusions of these studies were influenced by the use of different data sets and modeling approaches, though it is unlikely that consensus would have been achieved with more comprehensive analyses, as the resolution of the post-Landers deformation remains a limiting factor.

[4] The Landers earthquake was followed soon after by the nearby 1999 M7.1 Hector Mine quake (Figure 1). As the Hector Mine earthquake was of similar magnitude and sense of slip as Landers, and perturbed the same crust and mantle, one would expect a similar postseismic response. Unlike the Landers quake, however, postseismic deformation following the Hector Mine quake was recorded at an extensive array of continuous GPS stations that span a very broad region of southern California and into Nevada (more than 200 km from the epicenter). This first of a kind far-field view (over 4 rupture lengths) of a postseismic deformation field following a strike-slip earthquake, allows us to much more uniquely determine the mechanism responsible for this broad deformation pattern.

### 2. Observational Constraints and Modeling Approach

[5] We rely on daily time-series from continuously operating GPS sites, most of which are part of the SCIGN network that became operational between 1996 and 2001. The time-series are used to estimate horizontal and vertical components of linear interseismic displacement rates, coseismic offsets, and a logarithmically decaying function that represents the postseismic signal (see auxiliary material<sup>1</sup>). Seven years of cumulative transient deformation resolves a broad postseismic response (Figure 1, black arrows) to the 1999 M7.1

<sup>1</sup>Department of Earth and Atmospheric Sciences, Purdue University, West Lafayette, Indiana, USA.

<sup>2</sup>Department of Earth and Planetary Science, University of California Berkeley, Berkeley, California, USA.

<sup>3</sup>Department of Earth, Atmospheric, and Planetary Sciences, Massachusetts Institute of Technology, Cambridge, Massachusetts, USA.

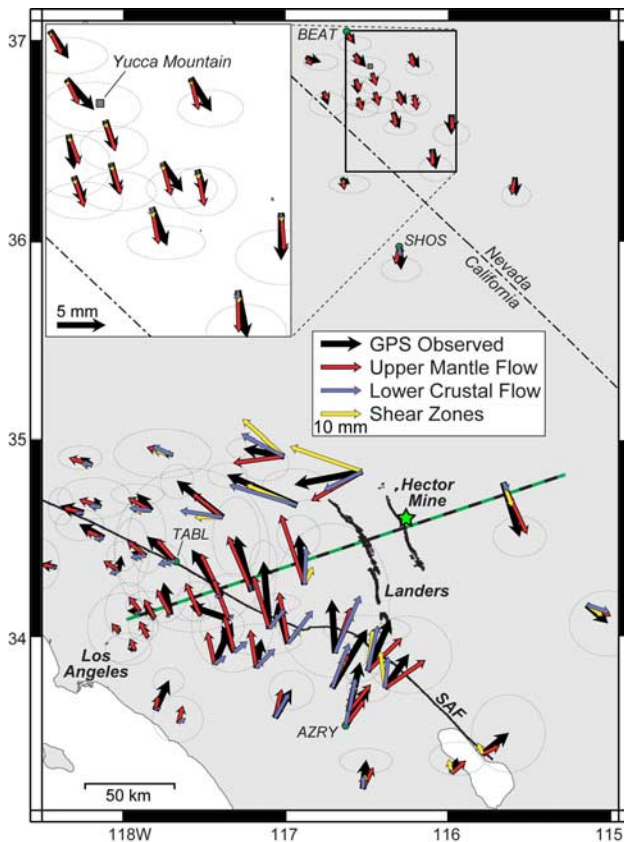


**Figure 1.** Cumulative GPS observed postseismic horizontal surface displacements (transient component) for the 7 year period following the 1999 Hector Mine earthquake compared to those calculated by models of viscoelastic flow and afterslip within narrow shear zones. Stations within 20 km of the Landers and Hector Mine rupture surfaces have been excluded from this comparison (see auxiliary material Figure S3 for near-field displacements). SAF: San Andreas Fault. Inset: Enlargement of Yucca Mountain region. GPS errors are shown at the 95% confidence level, as computed using a correlated noise model as described by Herring [2003]. See auxiliary material Table S1 for tabulated GPS data. Upper mantle viscosity structure is the blue line in Figure 2b. Lower crustal viscosity structure is the red line shown in Figure 2b. Green/black dashed line shows the apex of the curved deformation field to the southwest of the Landers rupture. Transient time-series of labeled stations are shown in auxiliary material Figure S1.

Hector Mine earthquake, as well as continued deformation from the nearby 1992 M7.3 Landers earthquake. The post-seismic response reaches the vicinity of Yucca Mountain, Nevada, more than 200 km from the Hector Mine epicenter (Figure 1, inset).

[6] To understanding the mechanism responsible for this deformation pattern we use a 3-D viscoelastic finite element model of the Mojave region that incorporates both rupture surfaces (auxiliary material Figure S2a). We use the inferred coseismic slip distribution of Fialko [2004b] for the Landers earthquake, and that of Simons *et al.* [2002] for the Hector Mine earthquake, as well as the same layered elastic structure (auxiliary material Figures S2b and S2c). For

every candidate rheology investigated (except poroelastic rebound for which we calculate an immediate cumulative response), we first simulate the Landers rupture, allow the rheology to respond to these stress changes for 7 years, then simulate the Hector Mine rupture and allow the rheology to respond for another 7 years. Calculated cumulative post-seismic model displacements over this latter 7-year period are compared to those observed to test each rheology.

### 3. Results

[7] We first consider models with a layered viscoelastic structure and seek to understand the depth of flow required to explain both far-field (i.e., in the region of Yucca Mountain; inset of Figure 1) and mid-field (remaining stations in Figure 1) surface displacements. Since shallow mechanisms, such as afterslip and poroelastic rebound [Jacobs *et al.*, 2002, Fialko, 2004a] contribute to near-field deformation (within 30 km), we do not consider near-field displacements (auxiliary material Figure S3) in best-fit calculations. In an initial sensitivity study, we allow viscoelastic flow to occur in only one narrow depth interval at a time, and solve for the viscosity required at each interval to best fit the observations based on a weighted sum of squared residuals (WSSR; Figure 2a). We find that viscoelastic relaxation in the lower crust (20–28 km depth) or uppermost mantle (28–40 km depth) leads to significant misfit, especially for far-field motions, compared to viscoelastic flow below a depth of 40 km, with misfit minimized between the depths of 40–56 km.

[8] The misfit induced by viscoelastic flow in the lower crust or uppermost mantle is large because flow in these depths leads to a wavelength of surface deformation that is shorter than the observed broad pattern. Considering a model of lower crustal flow (20–28 km depth) with a best-fit viscosity of  $1.2 \times 10^{18}$  Pa s. Figure 1 (blue arrows) shows that this model reasonably predicts mid-field displacements, but greatly underpredicts far-field displacements in the Yucca Mountain region (residual displacements are shown in auxiliary material Figure S4b). In addition, deformation predicted by lower crustal flow greatly underpredicts displacements along the apex of curvature (green/black dashed line in Figure 1).

[9] We considered a wide range of possible viscoelastic structures ranging from viscosity being uniform with depth below 20 km depth, to structures where viscosity decreases rapidly with depth (as might be expected due to increasing temperatures). Figure 2b shows a sample of tested viscosity structures along with calculated misfits. The best models (cyan and blue lines) are those where the viscosity below 40 km depth is an order of magnitude or more lower than the viscosity of mantle above and two orders of magnitude less than the viscosity of the lower crust. A model where flow occurs primarily below 63 km depth (black line) begins to introduce greater misfit, as below this depth coseismic stress changes are too small to drive significant flow. Displacements predicted by one of the best-fit models (blue line in Figure 2b), are shown in Figure 1 (red arrows; residual displacements are shown in auxiliary material Figure S4a). It is particularly impressive how well this upper mantle flow model predicts the displacements in the area of Yucca Mountain (even the rotation of azimuth

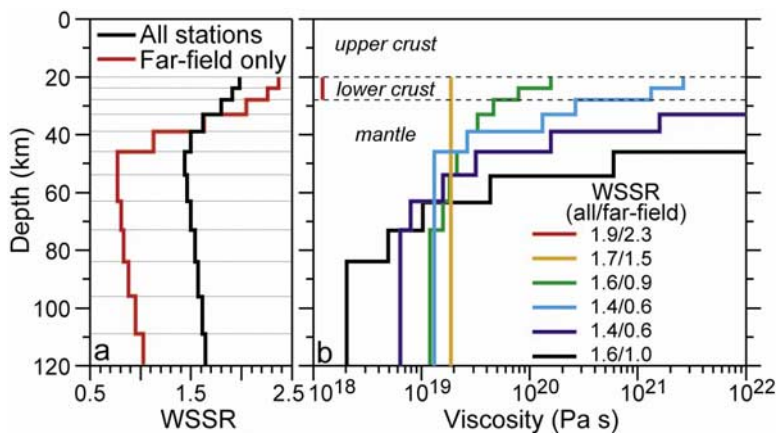


**Figure 2.** (a) Weighted misfit as a function of the depth interval (defined by thin gray lines) at which viscoelastic flow is allowed to occur (i.e. this is a composite of results from 12 models of flow at various depths). We quantify misfit (WSSR) as  $\sqrt{(1/m)\sum(d_o - d_c)^2/\sigma^2}$ , where  $d_o$  and  $d_c$  are the observed and calculated displacements,  $\sigma$  is the observational error, and  $m$  is the total number of observations. The viscosity values were tuned to match the observed displacements of “all stations” shown in Figure 1. Best-fit viscosity values decrease with depth from  $4.6 \times 10^{18}$  Pa s for the lower crustal layer from 20–24 km depth to  $4.0 \times 10^{17}$  Pa s for the region from 109–123 km depth. “Far-field only” refers to the misfit of these same models to just the far-field Yucca Mountain region stations (inset of Figure 1). (b) Viscosity versus depth profile for a variety of viscoelastic flow models considered. The viscosity of all models was tuned to match the observed displacements of all stations in Figure 1. Misfits are shown for calculations based on all stations (All) and for just the far-field Yucca Mountain stations (Far-field).

between northern and southern stations), while also matching the trend of deformation throughout southern California. It is worth noting that the best-fit model does not require consideration of lateral variations in viscosity structure despite the fact that the region encompasses several tectonic provinces. This may indicate that heterogeneities in crustal properties are not mirrored by heterogeneities in the mantle beneath, perhaps because the latter is mobile. The superiority of the upper mantle flow model compared to that of flow in the lower crust is also evident with observed vertical displacements (Figure 3).

[10] It should be noted that the viscosities shown in Figure 2 are average values over the 7 year time period that lead to the best fit with respect to the observed cumulative displacements. The Newtonian rheology used here cannot explain very rapid early postseismic displacements. Such behavior requires a rheology where effective viscosity increases with time, such as a Burgers [Pollitz, 2003] or power-law rheology [Freed and Bürgmann, 2004]. We experimented with a power-law rheology and found that though calculated postseismic displacement time-series evolve much differently from those resulting from Newtonian rheology, they produce similar surface deformation patterns (when the depth of flow is similar), and these patterns do not vary much with time.

[11] We can also rule out significant contributions of localized afterslip below the seismogenic zone to far-field postseismic deformation. We modeled afterslip by creating 3-km-wide shear zones in the mesh that extend downward from the base of the seismogenic zone through to the bottom of the model beneath both rupture surfaces. These zones extend to the north and south several hundreds of kilometers (green/black dashed lines in auxiliary material Figure S5), a likely overestimation of the lateral extent of such shear zones. The relaxation of coseismic stresses

within the shear zones is controlled by a viscoelastic rheology, with all volumes outside of this zone modeled as elastic. The maximum afterslip that can occur in the lower crust associated with the release of coseismic stresses is simulated by assigning a very low viscosity ( $10^{17}$  Pa s) to the shear zone between 20 and 28 km depth, which leads to complete relaxation of this region in the 7 year time frame of the postseismic observations. This model leads to surface displacements that are not significant beyond about 50 km from the rupture surfaces (Figure S5, blue arrows).

[12] Similarly, we can simulate the complete release of coseismic stress in a mantle shear zone below a depth of 28 km. This model leads to modest displacements in the far-field, ~20% of the displacements observed in the Yucca Mountain region (Figure S5, red arrows). Finally, we consider narrow shear zones that cut both the lower crust and mantle beneath the Landers and Hector Mine ruptures. This model leads to far-field postseismic displacement of ~22% of that observed and insignificant displacement in many mid-field locations (Figure 1, yellow arrows; residual displacements are shown in auxiliary material Figure S4d). Since the magnitudes of many of the other mid-field displacements are matched by the shear zone model, adding a component of mantle flow would lead to significant overshoot at these sites. Thus, afterslip within a localized shear zone below the seismogenic crust cannot be a significant source of the observed broad postseismic deformation pattern. To further quantify this result, we considered shear zones in the mantle ranging up to 400 km width. Only when the shear zone was large enough to incorporate the area beneath the Yucca Mountain region (~300 km width) did calculated far-field displacements approach the observed magnitude. Large postseismic far-field displacements beneath the Yucca Mountain region can only be explained by broad viscoelastic flow in the mantle.

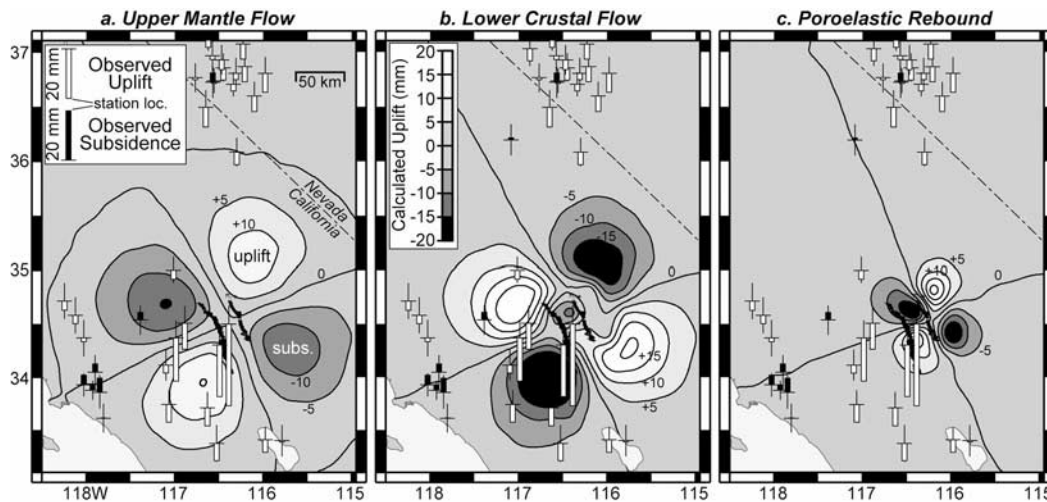


**Figure 3.** Cumulative GPS observed postseismic vertical surface displacements (white bars show uplift, black bars show subsidence) for the 7 year period following the 1999 Hector Mine earthquake compared to those calculated (contours) by models of viscoelastic flow in (a) the upper mantle (blue line viscosity structure in Figure 2b) and (b) the lower crust (red line in Figure 2b) and (c) poroelastic rebound. GPS errors are shown at the 68% confidence level. Stations with estimated errors greater than 5 mm in the 7-year span of the observations have been excluded from this comparison.

[13] We can also rule out a significant contribution to mid- and far-field postseismic displacements from poroelastic rebound. We use the same parameterization of poroelastic rebound employed by *Fialko* [2004a] to explain InSAR images following the Landers earthquake, to calculate the contribution of poroelastic rebound following the Hector Mine earthquake. We find horizontal surface displacements greater than 4 mm due to poroelastic rebound to be confined to within 50 km of the Hector Mine earthquake (auxiliary material Figure S3; residual displacements are shown in auxiliary material Figure S4c). Figure 3c shows that significant vertical displacements predicted by the poroelastic model are also confined to very near-field regions surrounding the Hector Mine rupture. While a poroelastic model does predict uplift to the southwest, it significantly underpredicts the observed uplift that is concentrated just beyond the reach of this mechanism.

#### 4. Discussion and Conclusions

[14] Previous postseismic studies have generally concentrated on relatively near-field displacements, usually with only a few observations beyond a rupture length. Such analyses have generally been plagued by trade-offs between different postseismic mechanisms and trade-offs between the depths at which these mechanisms operate. Like the present study, previous analyses have inferred a relatively weak mantle beneath the Mojave Desert [*Pollitz et al.*, 2000; *Pollitz*, 2003; *Freed and Bürgmann*, 2004], but those primarily near- and mid-field studies showed trade-offs with lower crustal flow. In contrast, this analysis of broad, far-field postseismic displacements observed throughout southern California and into Nevada following the Hector Mine earthquake requires a fairly unique solution; that flow be deep (below 40 km) and distributed across 100s of km. Specifically, there are no trade-offs to lower crustal flow or narrow shear zone mechanisms or poroelastic rebound to explain significant postseismic displacements observed in

the Yucca Mountain region, more than 200 km from the Hector Mine epicenter.

[15] It is important to note that the present study does not rule out the contribution of shallow afterslip and poroelastic rebound to influence postseismic displacements in the near-field, as suggested by previous analyses [e.g., *Peltzer et al.*, 1998; *Jacobs et al.*, 2002; *Fialko*, 2004a]. In fact, near-field displacements cannot be explained solely by mantle flow and require other mechanisms being active (auxiliary material Figure S4a). Near-field displacements do, however, contain a component from viscoelastic flow in the upper mantle (red arrows in auxiliary material Figure S3). Thus, analyses that do not take into account a contribution from viscoelastic flow in the mantle to near-field displacements [*Fialko*, 2004a; *Perfettini and Avouac*, 2007] are likely misinterpreting the postseismic observations.

[16] Our inference of a relatively weak mantle 40 km below the Mojave Desert is consistent with seismic velocities in the region that suggest a thin (order 10 km) mantle lid overlying a relatively hot, and likely convecting, asthenosphere [*Melbourne and Helmberger*, 2001]. A shallow, weak mantle is also consistent with thermal models derived from seismic tomography of western North America [*Goes and van der Lee*, 2002] and evidence of a shallow asthenosphere inferred from Mojave Desert xenoliths [*Farmer et al.*, 1995]. Our inferred viscosity structure of the crust and upper mantle in western Nevada is comparable to that derived from isostatic rebound patterns of Lake Lahontan shorelines ( $5 \times 10^{18}$  Pa s mantle under a much stronger crust [*Bills et al.*, 2007]). It is also consistent with a strong crust and thin mantle lid overlying shallow asthenosphere (in this case at 60 km depth) inferred from analysis of postseismic deformation following the 2002 Denali, Alaska earthquake [*Freed et al.*, 2006a, 2006b]. These findings suggest that at least in some backarcs or recent backarcs, the rheology is best described as a continuously strong, though thin, lithosphere overlying a weak asthenosphere, the so-called “crème brûlée” model [*Jackson*, 2002;

Burov and Watts, 2006]. Considering the broad region of mantle sampled by these studies, it is possible that such a model may be appropriate for much of western North America and southern Alaska [Hyndman et al., 2005; Dixon et al., 2004].

[17] **Acknowledgments.** CGPS data utilized in this study was provided by the SCIGN, BARGEN, UNAVCO and the International GNSS service networks. We thank the Scripps Institution of Oceanography Orbit and Permanent Array Center (SOPAC) for making available loosely constrained GPS products that we used in generating the GPS results presented here. We thank Eric Fielding and Paul Segall for helpful reviews.

## References

- Bills, B. G., K. D. Adams, and S. G. Wesnousky (2007), Viscosity structure of the crust and upper mantle in western Nevada from isostatic rebound patterns of the late Pleistocene Lake Lahontan high shoreline, *J. Geophys. Res.*, *112*, B06405, doi:10.1029/2005JB003941.
- Burov, E. B., and A. B. Watts (2006), The long-term strength of continental lithosphere: “Jelly sandwich” or “crème brûlée”?, *GSA Today*, *16*, doi:10.1130/1052-5173(2006)016.
- Chen, W.-P., and P. Molnar (1983), Focal depths of intracrustal and intraplate earthquakes and their implications for the thermal and mechanical properties of the lithosphere, *J. Geophys. Res.*, *88*, 4183–4214.
- Deng, J., M. Gurnis, H. Kanamori, and E. Hauksson (1998), Viscoelastic flow in the lower crust after the 1992 Landers, *Science*, *282*, 1689–1692.
- Dixon, J. E., T. H. Dixon, D. R. Bell, and R. Malservisi (2004), Lateral variation in upper mantle viscosity: Role of water, *Earth Planet. Sci. Lett.*, *222*, 451–467.
- Farmer, G. L., A. F. Glazner, H. G. Wilshire, J. L. Wooden, W. J. Pickthorn, and M. Katz (1995), Origin of late Cenozoic basalts at the Cima volcanic field, Mojave Desert, California, *J. Geophys. Res.*, *100*, 8399–8415.
- Fialko, Y. (2004a), Evidence of fluid-filled upper crust from observations of postseismic deformation due to the 1992  $M_w$ 7.3 Landers earthquake, *J. Geophys. Res.*, *109*, B08401, doi:10.1029/2004JB002985.
- Fialko, Y. (2004b), Probing the mechanical properties of seismically active crust with space geodesy: Study of the coseismic deformation due to the 1992  $M_w$ 7.3 Landers (southern California) earthquake, *J. Geophys. Res.*, *109*, B03307, doi:10.1029/2003JB002756.
- Freed, A. M., and R. Bürgmann (2004), Evidence of power-law flow in the Mojave Desert mantle, *Nature*, *430*, 548–551.
- Freed, A. M., R. Bürgmann, E. Calais, J. Freymueller, and S. Hreinsdóttir (2006a), Implications of deformation following the 2002 Denali, Alaska, earthquake for postseismic relaxation processes and lithospheric rheology, *J. Geophys. Res.*, *111*, B01401, doi:10.1029/2005JB003894.
- Freed, A. M., R. Bürgmann, E. Calais, and J. Freymueller (2006b), Stress-dependent power-law flow in the upper mantle following the 2002 Denali, Alaska, earthquake, *Earth Planet. Sci. Lett.*, *252*, 481–489.
- Goes, S., and S. van der Lee (2002), Thermal structure of the North American uppermost mantle inferred from seismic tomography, *J. Geophys. Res.*, *107*(B3), 2050, doi:10.1029/2000JB000049.
- Herring, T. A. (2003), MATLAB Tools for viewing GPS velocities and time-series, *GPS Solutions*, *7*, 194–199, doi:10.1007/s10291-003-0068-0.
- Hyndman, R. D., C. A. Currie, and S. P. Mazzotti (2005), Subduction zone backarcs, mobile belts, and orogenic heat, *GSA Today*, *15*, doi:10.1130/1052-5173.
- Jackson, J. (2002), Strength of the continental lithosphere: Time to abandon the jelly sandwich?, *GSA Today*, *12*, 4–10, doi:10.1130/1052-5173(2002)012<0004:SOTCLT>2.0.CO.
- Jacobs, A., D. Sandwell, Y. Fialko, and L. Sichoix (2002), The 1999 ( $M_w$  7.1) Hector Mine, California, earthquake: Near-field postseismic deformation from ERS interferometry, *Bull. Seismol. Soc. Am.*, *92*, 1433–1442.
- Masterlark, T., and H. F. Wang (2002), Transient stress-coupling between the 1992 Landers and 1999 Hector Mine, California, earthquakes, *Bull. Seismol. Soc. Am.*, *92*, 1470–1486.
- Melbourne, T., and D. Helmberger (2001), Mantle control of plate boundary deformation, *Geophys. Res. Lett.*, *28*, 4003–4006.
- Peltzer, G., P. Rosen, F. Rogez, and K. Hudnut (1998), Poroelastic rebound along the Landers 1992 earthquake surface rupture, *J. Geophys. Res.*, *103*, 30,131–30,145.
- Perfettini, H., and J.-P. Avouac (2007), Modeling afterslip and aftershocks following the 1992 Landers Earthquake, *J. Geophys. Res.*, *112*, B07409, doi:10.1029/2006JB004399.
- Pollitz, F. F. (2003), Transient rheology of the uppermost mantle beneath the Mojave Desert, California, *Earth Planet. Sci. Lett.*, *215*, 89–104.
- Pollitz, F. F., G. Peltzer, and R. Bürgmann (2000), Mobility of continental mantle: Evidence from postseismic geodetic observations following the 1992 Landers earthquake, *J. Geophys. Res.*, *105*, 8035–8054.
- Shen, Z. K., et al. (1994), Postseismic deformation following the Landers earthquake, California, 28 June 1992, *Bull. Seismol. Soc. Am.*, *84*, 780–791.
- Simons, M., Y. Fialko, and L. Rivera (2002), Coseismic deformation from the 1999  $M_w$  7.1 Hector Mine, California, Earthquake as Inferred from InSAR and GPS Observations, *Bull. Seismol. Soc. Am.*, *92*, 1390–1402.

R. Bürgmann, Department of Earth and Planetary Science, University of California, Berkeley, CA 94720, USA.

A. M. Freed, Department of Earth and Atmospheric Sciences, Purdue University, 550 Stadium Mall Drive, West Lafayette, IN 47907, USA. (freed@purdue.edu)

T. Herring, Department of Earth, Atmospheric, and Planetary Sciences, Massachusetts Institute of Technology, Cambridge, MA 02139, USA.